Islamic Azad University

Journal of

Optoelectronical Nanostructures

Winter 2021 / Vol. 6, No. 1

Adsorption Behaviour of *CO* Molecule on $Mg_{16}M—O_2$ Nanostructures (*M=Be, Mg,* and *Ca*): A DFT Study

Mahmood Reza Dehghan[1], Sara Ahmadi[*,1]

[1] Department of Chemistry, Firoozabad Branch, Islamic Azad University, Firoozabad, Iran

(Received 11 Dec. 2020; Revised 20 Jan. 2021; Accepted 14 Feb. 2021; Published 15 Mar. 2021)

Abstract: In this study, density functional theory (DFT) calculations were performed to investigate the adsorption of *CO* molecule (via *O* and *C* atoms) on the surface of $Mg_{16}M—O_2$ (*M=Be, Mg,* and, *Ca*) nanostructures, *M* is the central atom, at the CAM-B3LYP/6-311+g(d) level of theory. The electronic properties of $Mg_{16}M—O_2$ nanostructures were significantly affected by the adsorption of the *CO* molecule. The NBO analysis revealed a charge transfer from the adsorbed *CO* molecule to the $Mg_{16}M—O_2$ nanostructure. Based on the adsorption energies and enthalpies, a thermodynamically favorable chemisorption process was predicted. The adsorption and binding energy values of the *CO* molecule (via both *O* and *C* atoms) over the $Mg_{16}M—O_2$ nanostructures have increased with increasing the atomic radius of the central atom in the nanostructures through a chemical and exothermic reaction. The $Mg_{16}CaO_2$—*CO* complex with the smallest bond distance and the largest adsorption energy shows the most tendency to adsorb carbon monoxide molecule.

Keywords: Adsorption, Carbon Monoxide, DFT, Electron Properties, Magnesium Nanostructure

1. INTRODUCTION

Metal clusters have been considered as novel physical materials with tremendous properties nearly two decades ago [1]. They illustrate several unprecedented non-monotonous size-dependent behaviors which are remarkably distinct from those of either isolated atoms or the bulk metal [2]. Divalent metal clusters with filled electronic shells have certain aspects of the van der Waals type of bonding between the atoms. Hence, they are expedient to study nonmetal to metal transition, examine various theoretical methodologies and perceptual extension of atomic cluster physics. Among divalent metal clusters, interest in magnesium clusters has grown dramatically in the past few decades because of a wide range of attractive properties such as high-temperature stability, low

[*] Corresponding author. Email: **s.ahmadi@iauf.ac.ir**

dielectric constant, large thermal conductivity, strong chemical reactivity and oxidation resistance [1, 3-5]. These properties lead to several diverse potentials such as superconductivity [6], hydrogen storage [7, 8], nanomaterials [9, 10], and biomedicine [11]. Apart from these valuable characteristics, magnesium clusters display the transition from weak van der Waals bonding to metallic bonding as the clusters grow in size [12]. A wide range of theoretical studies has been completed on the geometrical structures and electronic properties of the magnesium clusters [2, 5, 13-17]. Xia and *et al.* investigated the structural and electronic properties of neutral and anionic magnesium clusters with different sizes ranging from n=3 to 20, through combining a systematic exploration of the potential energy surface using CALYPSO [18] and density functional theory (DFT) calculations [17]. Subsequently, they indicated that the ground state structure of the neutral Mg_{17} cluster which contains two square Mg_4 frameworks can be considered as π-aromatic. Moreover, the Mg_{17} cluster is a 34 electrons system, which possesses a closed electronic shell according to the jellium super-atom Model [19, 20]. Therefore, due to the high potential of the Mg_{17} cluster, this study was implemented to further continue our probe on the capability of this cluster for adsorbing the different diatomic molecules. Carbon monoxide (*CO*) is a highly poisonous gas in low concentrations [21] but its package is used in various industries for a range of demands including metal fabrication, chemicals, steel and metals, electronics, pharma, and biotechnology [22-24]. However, a key problem is their storage thus; the inventing a portable, fast response, highly sensitive, easy to use, and reliable sensor to detect or adsorb *CO* molecule from the air is highly essential. The spectrophotometric, electrochemical, and gas chromatographic approaches [25-27] are some of the common techniques used to sense these gases which are time consuming and occasionally too complicated. With the advent of nanotechnology, the development of the gas sensors with high sensitivity and selectivity, adsorption capacity, high surface/volume ratio, and unique electronic sensitivity of nanostructures [28] has accelerated. Therefore, numerous nanostructured material based sensors have been introduced and investigated for different gases both experimentally and theoretically [29-34]. During the past few decades, density functional theory (DFT) has been frequently used to study a wide variety of properties of metal clusters [13, 17, 33-42]. In this study, we examine the possibility of the adsorption of *CO* molecule over the outer surface of $Mg_{16}M—O_2$ nanostructures (*M=Be, Mg* and *Ca*) in the gas phase using density functional theory (DFT) calculations. DFT is the most precise and reliable method to investigate metal nanocluster properties [35-40, 43, 44]. The natural bond orbital (NBO) analysis [45, 46] was used to interpret the charge transfer process between *CO* molecule and $Mg_{16}M—O_2$;(*M=Be, Mg,* and, *Ca*) during the adsorption process. The atoms in molecules

(AIM) approach was used to characterize the nature of the interactions by AIM2000 software [47].

2. Theoretical Methods

To investigate the *CO* adsorption (via *O* and *C* atoms) on the magnesium nanoclusters ($Mg_{16}Be$, $Mg_{16}Mg$, and, $Mg_{16}Ca$), the geometry of neutral magnesium nanoclusters consisting of 17 atoms with the atomic center of beryllium, magnesium, and calcium are modeled using Gauss View 5.0 [48]. We applied a filled-cage-like construction, including two square Mg_4 scaffolds (4-MRs) and an octagon scaffold (8-MR), (Fig. 1, part a) where stabilized in $Mg_{16}M$ because of the potent interactions between the Mg_4 units and the central *M* atom and more significantly due to the tendency of local aromaticity [17]. In our previous work, we investigated the adsorption of the uni-O_2 molecule on the surface of the $Mg_{16}Be$, $Mg_{16}Mg$, and, $Mg_{16}Ca$ nanoclusters [49]. The optimized energy values of the O_2 adsorption indicated the 4-MRs frames are more desirable for O_2 adsorption in three nanoclusters of $Mg_{16}Be$, $Mg_{16}Mg$, and, $Mg_{16}Ca$. Consequently, in this study, we intend to investigate the adsorption of *CO* molecule (via *O* and *C* atoms) over the outer surface of $Mg_{16}M—O_2$ (4-MRs) nanostructures (*M=Be, Mg* and *Ca*) to understand the adsorption behavior of $Mg_{16}M$;(*M=Be, Mg,* and, *Ca*) toward different molecules. The adsorption position for the *CO* molecule on the $Mg_{16}M—O_2$ complexes were determined through charge analysis (natural bond orbital analysis, (NBO)) of the optimized complexes of $Mg_{16}M—O_2$ $(M = Be, Mg\ and, Ca)$. For this purpose, we determine the charge of each *Mg* atom of the most stable complex and the *Mg* atom with the highest negative and positive charge was selected for adding the *CO* molecule through *C* and *O* atom respectively. All structures were geometrically optimized using the hybrid exchange–correlation functional CAM-B3LYP which combines the hybrid qualities of B3LYP and the long-range correction presented by Tawada *et al.* [50] and 6-311+g(d) basis set in the gas phase using the Gaussian 09 package [51]. Normal mode frequency analysis was performed numerically from the analytical gradients. The absence of negative frequency in normal mode analysis indicates the optimized structure on the potential energy surfaces (PES) were real minimum stationary points. The adsorption energies of the studied complexes are corrected separately, for both ZPE and basis set superposition error (BSSE) using the counterpoise correction scheme outlined by Boys and Bernardi [52].

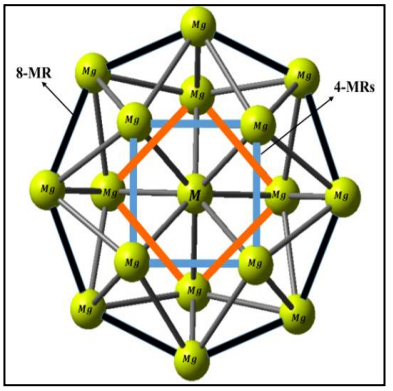

a) $Mg_{16}M$ $(M = Be, Mg\ and, Ca)$ nanocluster

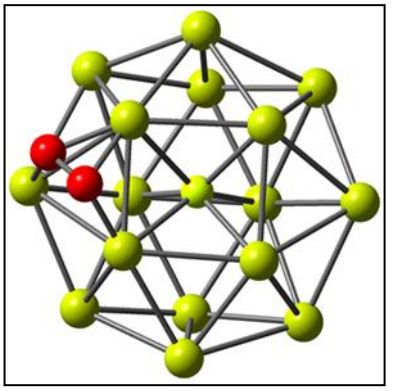

b) *Mg16Be—O2* (4-MRs) complex

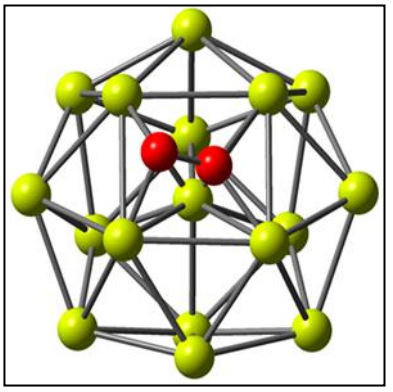

c) *Mg16Mg—O2* (4-MRs) complex

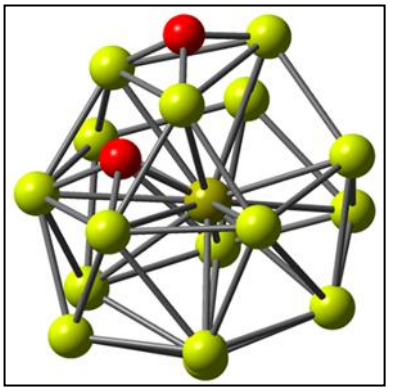

d) *Mg16Ca—O2* (4-MRs) complex

Fig. 1. (a) Schematic view of the $Mg_{16}M(M = Be, Mg\ and, Ca)$ nanoclusters, the blue and red bonds represent the two 4-membered rings (4-MRs) and the thick black bonds represent one 8-membered ring (8-MR), M is the central atom (*M=Be, Mg,* and, *Ca*). (b), (c), and, (d) are the optimized structures of the uni-molecular O_2 adsorption of *$Mg_{16}M—O_2$ (M=Be, Mg, and, Ca)* at the CAM-B3LYP/ 6-311+G(d) level of theory in our previous prob.

Furthermore, using the obtained results from the calculations, the structural and electronic properties and also the thermodynamic parameters were calculated. The density of state (DOS), and the partial density of state (PDOS) were obtained for all adsorption models using the Gauss Sum [53] and Multiwfn [54] programs. The EDD maps were generated by VMD software.

3. Results and Discussion

3.1. The Adsorption of CO Molecule on the Surface of Mg16M—O_2 (M=Be, Mg, and Ca) Nanostructures

The interaction energies of the *CO* adsorption on the studied nanostructures were calculated to determine the adsorption behavior of this molecule upon the exterior surface of the investigated nanostructures. The adsorption energy (E_{ad}), binding energy (E_{bind}) and deformation energy (E_{def}) are calculated based on following equations:

$$Mg_{16}M—O_2 + X \rightarrow Mg_{16}M—O_2 \ldots X \qquad M = Be, Mg, Ca \quad X = CO, OC$$

$$E_{ad} = E_{Mg_{16}M—O_2 \ldots X} - (E_{Mg_{16}M—O_2} + E_X) \tag{1}$$

$$E_{bind} = E_{Mg_{16}M—O_2 \ldots X} - (E_{Mg_{16}M—O_2\ in\ complex} + E_{X\ in\ complex}) \tag{2}$$

$$E_{def} = E_{ad} - E_{bind} \tag{3}$$

Where $E_{Mg_{16}M—O_2}$ and $E_{Mg_{16}M—O_2 \ldots X}$ are the optimized energies of different complexes. To study the *CO* adsorption (via both *O* and *C* atoms) over the $Mg_{16}M—O_2$ nanostructure, we used the most stable nanostructures of $Mg_{16}M—O_2$ (*M=Be, Mg* and, *Ca*) in our previous study, and added a carbon monoxide molecule (via both O and C atoms) on these nanostructures. As a result, we have studied six distinct starting structures which includes three cases of approaching *CO* molecule via its carbon atom to the most negative *Mg* atom of the $Mg_{16}M—O_2$ (*M=Be, Mg* and, *Ca*) nanostructures and three cases via its oxygen atom to the most positive *Mg* atom of the $Mg_{16}M—O_2$ (*M=Be, Mg* and, *Ca*) nanostructures.
Table 1 illustrates the calculated values of the binding distance (*R*), adsorption energy (E_{ad}), binding energy (E_{bind}), and deformation energy (E_{def}) for the $Mg_{16}MO_2—CO$ and $Mg_{16}MO_2—OC$ complexes at the CAM-B3LYP/6-311+g(d) level of theory. The adsorption and binding energy values of the *CO* molecule (via both *O* and *C* atoms) over the $Mg_{16}M—O_2$ nanostructures have increased with increasing the atomic radius of the central atom in the nanostructures through a chemical and exothermic reaction. As such, the highest adsorption energy observed for $Mg_{16}CaO_2—CO$ and $Mg_{16}CaO_2—OC$ with -297.5009 and -289.7590 kcal/mol, respectively and the binding energy values, vary from -189.8811 to -525.0410 kcal/mol for $Mg_{16}BeO_2—OC$ to $Mg_{16}CaO_2—CO$ respectively. As mentioned in section 3.1, the stability of the $Mg_{16}M—O_2$ (*M=Be, Mg,* and, *Ca*) nanostructures decrease with increasing the radius of the central atom therefore, the reactivity will increase. As a result, the $Mg_{16}Ca—O_2$ nanostructure shows the highest adsorption energy during the *CO* (via both *O* and *C* atoms) adsorbing.

Table 1. The calculated adsorption energy (E_{ad}), binding energy (E_{bind}) and deformation energy (E_{def}) all in (kcal/mol), binding distance (R) (Å) for the $Mg_{16}MO_2$—CO and $Mg_{16}MO_2$—OC complexes, at the CAM-B3LYP/6-311+g(d) level of theory.

complex	Adsorption position	R(Å)	E_{ad}	E_{bind}	E_{def}
$Mg_{16}BeO_2$—CO	a*	2.32	-140.6290	-192.9501	+52.3211
$Mg_{16}MgO_2$—CO	a	2.26	-273.3701	-349.9412	+76.5711
$Mg_{16}CaO_2$—CO	a	2.25	-297.5009	-525.0410	+227.5401
$Mg_{16}BeO_2$—OC	b*	3.54	-136.9398	-189.8811	+52.9413
$Mg_{16}MgO_2$—OC	b	4.01	-266.1607	-342.1121	+75.9514
$Mg_{16}CaO_2$—OC	b	3.46	-289.7590	-516.9501	+227.1911

**a and b; related to the atom with the most negative and positive charge in the complex respectively.*

It should be noted that, the electronegativity of the central atom plays an important role during the adsorptions of carbon monoxide on different nanostructures. Hence, calcium as the central atom with the least electronegativity induces strong role in carbon monoxide adsorption. The interaction energy values of the investigated systems anticipate the chemisorption process for adsorbing carbon monoxide molecule on the surface of the nanostructures. Additionally, the deformation energy values vary from 52.3211 to 227.5401 kcal/mol for $Mg_{16}BeO_2$—CO to $Mg_{16}CaO_2$—CO respectively, which indicates a significant deviation in the geometry of these nanostructures during the adsorption of the CO molecule. It assumed that during the adsorption of carbon monoxide, an electron transfer occurs between the carbon monoxide and the nanostructure surface, therefore, a significant curvature with the large values of deformation energy was observed (see Table 1). The NBO analysis indicates a depletion of the electron from CO molecule to the $Mg_{16}Ca$—O_2 nanostructure results in an improvement in the adsorption of carbon monoxide and also an increase in the interaction energy. Consequently, for the most stable adsorbed model ($Mg_{16}CaO_2$—CO) a high charge of 0.13513 e is transferred from CO molecule to the $Mg_{16}Ca$—O_2 nanostructure. The corresponding EDD isosurfaces also confirm a redistribution pronounced electron density over the CO and $Mg_{16}Ca$—O_2 nanostructure. In addition, there is a great electron density accumulation around the Mg—C bond, which confirms the strong chemical adsorption of CO over the $Mg_{16}Ca$—O_2 nanostructure surface (Fig. 2).

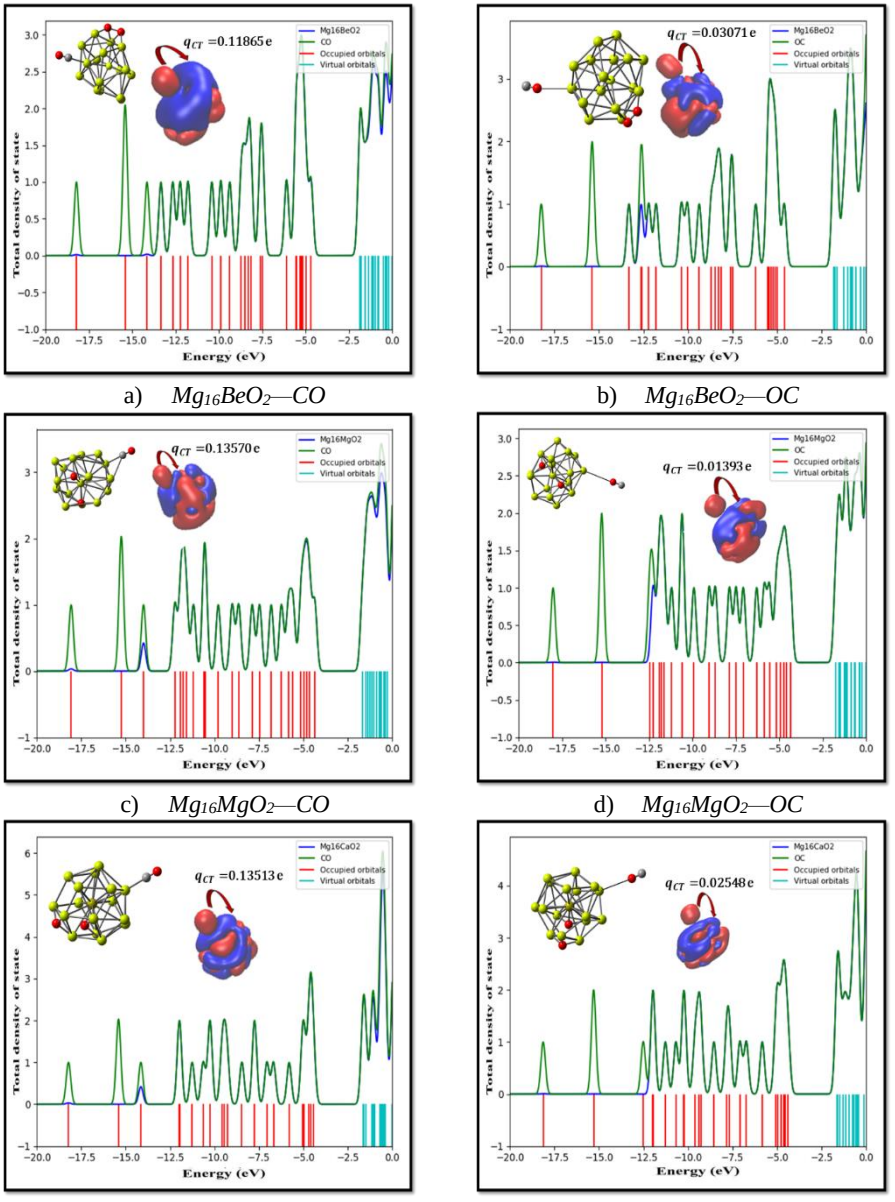

Fig. 2. The optimized structures of the different complexes $Mg_{16}MO_2$—*CO* and $Mg_{16}MO_2$—*CO* at the CAM-B3LYP/ 6-311+G(d) level of theory along with their corresponding EDD maps (0.001 au) and PDOS plots. In the EDD maps, the electron density depletion and accumulation sites are displayed in red and blue, respectively. q_{CT} indicates the charge transfer.

3.2. Atoms in Molecules (AIM) Analysis

Bader's theory of atoms in molecules (AIM) is a powerful method to study the nature of the interactions [55] via parameters, such as electron density, $\rho_{(r)}$ the Laplacian of the electron density, $\nabla^2{}_{\rho_{(r)}}$ and the ellipticity (ε), which are computed at the bond critical point (BCP). According to this theory, when two neighboring atoms are chemically bonded, a bond critical point appears between the acceptor and donor atoms. At the bond critical point, the Laplacian of the charge density $\nabla^2{}_{\rho_{(r)}}$, is the sum of the curvature in the charge density along any orthogonal coordinate axes [56]. Negative values for Laplacian of the electron density ($\nabla^2{}_{\rho_{(r)}} < 0$) reveal that the charge density is concentrated, as the covalent bond and positive values ($\nabla^2{}_{\rho_{(r)}} > 0$) show a depleted charge density, a sign closed-shell (electrostatic) interactions [57, 58].

Table 2. Topological parameters, the electron density $\rho_{(r)}$, Laplacian of the electron density $\nabla^2{}_{\rho_{(r)}}$, Ellipticity (ε) and energetic parameters for the *Mg—O* and *Mg—C* at the bond critical points (BCPs); electronic potential energy density, $V_{(r)}$, electronic kinetic energy density, $G_{(r)}$ and electronic energy density $H_{(r)}$ all in (a.u.) for the studied systems, at the CAM-B3LYP/6-311+G(d) level of theory.

complex	$\rho_{(r)}$	$\nabla^2{}_{\rho_{(r)}}$	ε	$G_{(r)}$	$V_{(r)}$	$H_{(r)}$
$Mg_{16}BeO_2$—CO	0.02607	0.13439	0.05208	0.03005	0.02650	0.05655
$Mg_{16}MgO_2$—CO	0.02877	0.15854	0.02891	0.03520	0.03077	0.06597
$Mg_{16}CaO_2$—CO	0.02925	0.16127	0.05833	0.03576	0.31200	0.06696
$Mg_{16}BeO_2$—OC	0.00275	0.00563	0.12544	0.00121	0.00101	0.00222
$Mg_{16}MgO_2$—OC	0.00141	0.00337	0.18761	0.00064	0.00045	0.00109
$Mg_{16}CaO_2$—OC	0.00337	0.00501	0.12014	0.00105	0.00085	0.00190

To analyze the characteristics of the bond critical points at the interaction sites of carbon monoxide molecule on the *$Mg_{16}M$—O_2* nanostructures, the values of the electron density, Laplacian of the electron density, ellipticity, density of the total energy of electrons ($H_{(r)}$) and its two components, kinetic ($G_{(r)}$) and potential ($V_{(r)}$) electron energy densities for all investigated compounds have been calculated and tabulated in Table 2. For all studied complexes, the Laplacian of the total electron densities at BCPs of *Mg—O* and *Mg—C* bonds are positive and reveal that electronic charges are depleted in the interatomic path, which is characteristic of the closed-shell interactions. The interaction behavior can be classified as a function of $H_{(r)}$ and the Laplacian of the electron density at BCP [59]. For strong interaction ($\nabla^2{}_{\rho_{(r)}} < 0$ and $H_{(r)} < 0$), the covalent character is

established; for medium strength ($\nabla^2{}_{\rho_{(r)}} > 0$ and $H_{(r)} < 0$), the partially covalent character is defined; and weak ones with $\nabla^2{}_{\rho_{(r)}} > 0$ and $H_{(r)} > 0$ are mainly electrostatic interaction. As such, the interactions between all the studied complexes have an electrostatic character in nature, due to the positive values of $\nabla^2{}_{\rho_{(r)}}$ and $H_{(r)}$. In addition, our theoretical results show that in all of the investigated systems $G_{(r)} > 0$ and $V_{(r)} > 0$. Table 2 reveals the $Mg_{16}CaO_2$—*CO* and $Mg_{16}CaO_2$—*OC* complexes have the smallest intermolecular distances (2.25 and 3.46 Å respectively) and highest electron density of 0.02925 and 0.00337 a.u. respectively, which clarify the electrostatic features in these complexes. These results are in good agreement with the large binding energies obtained for these complexes. Furthermore, the analysis of the electron density for the studied complexes indicates the electron density at the BCP will increase with the enhancement of the interaction energy. The calculated electron density properties (Table 2) illustrate among different complexes, the $Mg_{16}CaO_2$—*CO* with the value of $\rho_{(r)}$=0.02925 is the most stable complex for adsorbing the molecule of *CO*.

3.3. Electronic properties

The remarkable contribution in the chemical stability and chemical reactivity is related to the frontier orbitals of the highest occupied molecular orbital energies (HOMO) and lowest unoccupied molecular orbital energies (LUMO) which illustrate the electron-donating and accepting ability, respectively [60]. The evaluation of the transition energy from HOMO to LUMO (energy gap; E_{gap}) was carried out to measure the molecular reactivity and evaluation of the sensitivity of each nanostructure relative to the *CO* molecule. Table 3 illustrates the values of the ε_{HOMO} and ε_{LUMO}, energy gap (E_{gap}), chemical potential (μ), chemical hardness (η) and, electronegativity (χ) for the studied complexes. The chemical reactivity of the investigated nanostructure can be characterized by calculating the energy gap which is a significant parameter relying on the HOMO and LUMO energy levels. A large gap, corresponds to high stability and a small gap shows low stability. In turn, the high stability is associated with the low chemical reactivity and the small stability has high chemical reactivity [61, 62]. It can be seen that the optimized $Mg_{16}Ca$—O_2 nanostructure shows a smaller gap than $Mg_{16}Mg$—O_2 and $Mg_{16}Be$—O_2 nanostructure at the CAM-B3LYP level of theory. Consequently, the $Mg_{16}Ca$—O_2 nanostructure has the most chemical reactivity compared to the other nanostructure. Moreover, Table 3 shows the HOMO–LUMO energy gap (E_{gap}) values for *CO* adsorption over the $Mg_{16}M$—O_2 (*M =Be* and *Ca*) increased compared to their pristine nanostructure, leading to

more stability for complexes of $Mg_{16}Be—O_2$ and $Mg_{16}Ca—O_2$. Whilst, the *CO* adsorption upon the $Mg_{16}Mg—O_2$ causes a decrease in the HOMO–LUMO energy gap from 2.7919 eV to 2.6842 eV and 2.6207 eV for $Mg_{16}MgO_2—CO$ and $Mg_{16}MgO_2—OC$, respectively. This leads to instability for complexes of $Mg_{16}MgO_2—CO$ and $Mg_{16}MgO_2—OC$.

Table 3. The energy of HOMO (ε_{HOMO}), LUMO (ε_{LUMO}), gap energiy (E_{gap}), chemical potential (μ), chemical hardness (η), and electronegativity (χ) (all in eV) for the studied compounds, at the CAM-B3LYP/6-311+g (d) approach.

structure	ε_{HOMO}	ε_{LUMO}	E_{gap}	$\Delta\varepsilon_g\%$	μ	η	χ
$Mg_{16}Be—O_2$	-4.6123	-1.8476	+2.7647	—	-3.2311	+1.3823	+3.2311
$Mg_{16}BeO_2—CO$	-4.6784	-1.8675	+2.8109	+1.67	-3.2729	+1.4055	+3.2729
$Mg_{16}BeO_2—OC$	-4.5935	-1.8221	+2.7714	+0.24	-3.2078	+1.3857	+3.2078
$Mg_{16}Mg—O_2$	-4.6205	-1.8286	+2.7919	—	-3.2247	+1.3966	+3.2247
$Mg_{16}MgO_2—CO$	-4.3541	-1.6699	+2.6842	-3.86	-3.0120	+1.3407	+3.0120
$Mg_{16}MgO_2—OC$	-4.3616	-1.7409	+2.6207	-6.13	-3.0514	+1.3104	+3.0514
$Mg_{16}Ca—O_2$	-4.3946	-1.6572	+2.7374	—	-3.0279	+1.3689	+3.0279
$Mg_{16}CaO_2—CO$	-4.4235	-1.6471	+2.7764	+1.43	-3.0353	+1.3882	+3.0353
$Mg_{16}CaO_2—OC$	-4.3796	-1.6414	+2.7382	+0.03	-3.0105	+1.3691	+3.0105

The global indices of reactivity in the context of DFT are represented in Table 3. Chemical hardness [63-65] is a measure of the resistance of a chemical species to change its electronic configuration, while electronic chemical potential measures the escaping tendency of an electron cloud. With the Mulliken definition for chemical potential, the negative μ values correlate to the more stable or less reactive compound. Therefore, $Mg_{16}Be—O_2$ nanostructure with μ= -3.2311 eV and $Mg_{16}Ca—O_2$ nanostructure with μ= -3.0279 eV have the least and most reactivity, respectively. On the other hand, the evaluated values of chemical hardness, are in a contrary relation with the values of the chemical potential. The hardness values of $Mg_{16}CaO_2—CO$ and $Mg_{16}CaO_2—OC$ complexes and also $Mg_{16}BeO_2—CO$ and $Mg_{16}BeO_2—OC$ complexes are significantly increased compared to their pristine nanostructures ($Mg_{16}Ca—O_2$ and $Mg_{16}Be—O_2$) which prove much less reactivity for these systems. Subsequently, to verify the effects of the adsorption of *CO* on the electronic properties of the studied systems, the electronic densities of states (DOSs) of these complexes have been calculated and tabulated in Fig. 3. More inspection of the DOS plots reveals that for $Mg_{16}MgO_2—CO$ and $Mg_{16}MgO_2—OC$ complexes, the conduction levels shift toward the lower energies compared to those of the pristine nanostructures. In contrast, for other complexes, the conduction levels shift toward the higher energies compared to those of the pristine nanostructures.

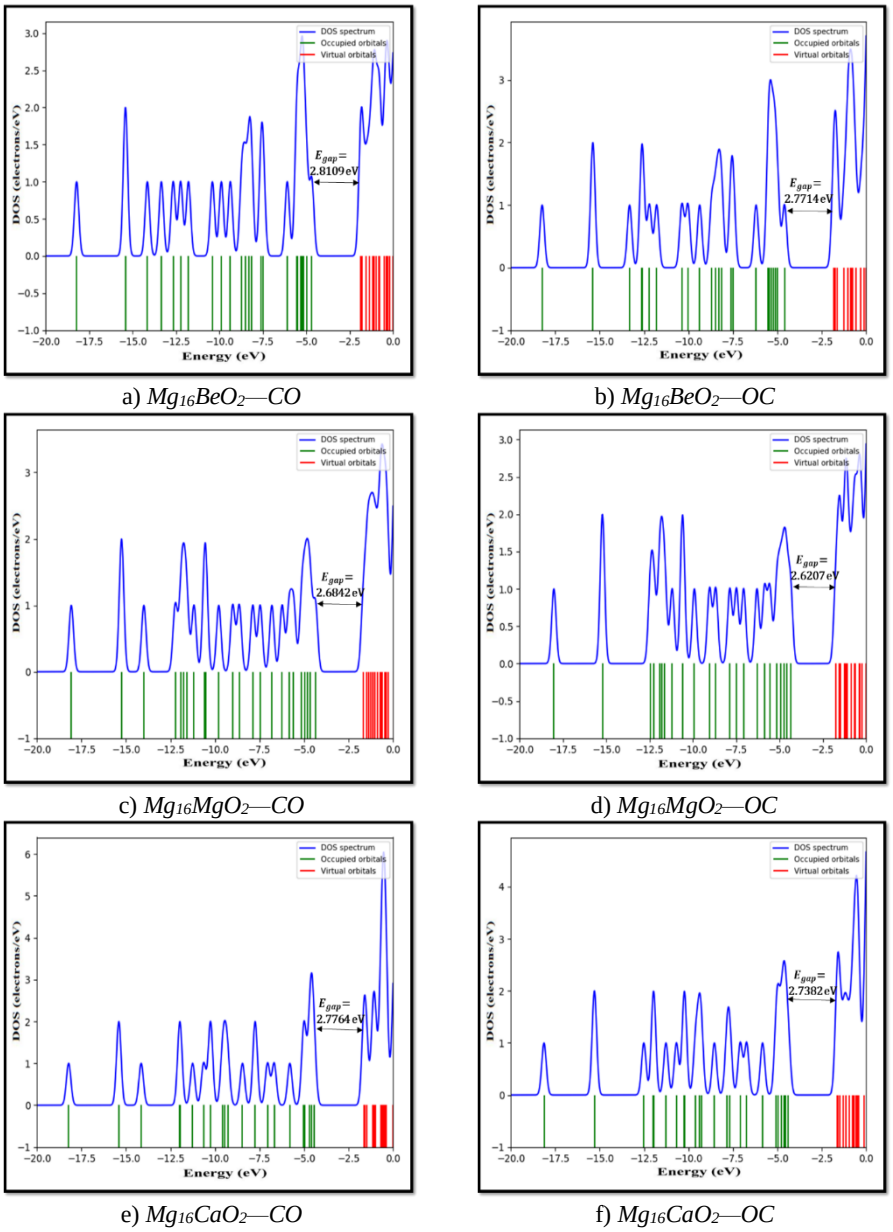

a) $Mg_{16}BeO_2$—CO b) $Mg_{16}BeO_2$—OC

c) $Mg_{16}MgO_2$—CO d) $Mg_{16}MgO_2$—OC

e) $Mg_{16}CaO_2$—CO f) $Mg_{16}CaO_2$—OC

Fig. 3. The illustration of the electronic density of states (DOS) for the studied complexes. The E_{gap} indicates the HOMO–LUMO energy gap.

3.4 Thermodynamic parameters

Thermodynamic parameters provide deep evidence of the essential energetic changes associated with the adsorption process. Table 4 summarizes the changes of the enthalpy (ΔH°), entropy ($T\Delta S^{\circ}$), and the Gibbs free energy (ΔG°) of the studied complexes at 298 K and 1 atmosphere. The calculated standard enthalpies predicted an exothermic adsorption process for the investigated complexes. The standard enthalpies of the adsorption process reduce by increasing the atomic radius of the central atom. On the other hand, the negative values of ΔG° for the studied complexes verify the spontaneous adsorption process. As a result, the $Mg_{16}CaO_2$—*CO* complex with the lowest relative standard Gibbs free energy of formation is the most thermodynamically stable.

Table 4. The calculated thermodynamic properties; standard enthalpy (ΔH°), standard entropy ($T\Delta S^{\circ}$) and standard Gibbs free energy (ΔG°) all in (kcal.mol^{-1}) and electronic properties; chemical potential (μ), chemical hardness (η) and electronegativity (χ) all in (eV) for studied complexes, at the CAM-B3LYP/6-311+g(d) approach.

structure	ΔH°	ΔG°	$T\Delta S^{\circ}$
$Mg_{16}BeO_2$—*CO*	-139.0020	-118.3977	-20.6043
$Mg_{16}BeO_2$—*OC*	-135.4025	-120.5236	-14.8789
$Mg_{16}MgO_2$—*CO*	-271.6435	-249.3743	-22.2692
$Mg_{16}MgO_2$—*OC*	-264.5385	-248.1953	-16.3432
$Mg_{16}CaO_2$—*CO*	-295.7576	-272.0373	-23.7203
$Mg_{16}CaO_2$—*OC*	-288.1573	-269.2906	-18.8667

4. Conclusion

The CAM-B3LYP/6-311+g(d) method was employed to investigate the interaction between the *CO* molecule and the $Mg_{16}M$—O_2 (*M=Be, Mg,* and, *Ca*) nanostructures, *M* is the central atom, in the gas phase. Based on the negative values of the Gibbs free energy, adsorption energies, and enthalpies, a spontaneous favorable adsorption process was predicted for CO adsorption on three studied complexes. The highest adsorption energy was observed for the $Mg_{16}CaO_2$—*CO* complex at the CAM-B3LYP level of theory, which causes a high charge transfer of 0.13513 e from *CO* molecule to the $Mg_{16}Ca$—O_2 nanostructure. Furthermore, the adsorption energy values of the *CO* molecule (via

both *O* and *C* atoms) over the $Mg_{16}M—O_2$ nanostructures have increased with increasing the atomic radius of the central atom in the complexes through a chemical and exothermic reaction. In summary, the $Mg_{16}M—O_2$ nanostructures with different central atom of *Be*, *Mg*, and *Ca* are likely candidates for storage the *CO* molecule, while $Mg_{16}Ca—O_2$ have the highest capacity to use as a reservoir for the adsorption of this gas.

REFERENCES

[1] A. Lyalin, I.A. Solov'yov, A.V. Solov'yov, W. Greiner, *Evolution of the electronic and ionic structure of Mg clusters with increase in cluster size*. Phys. Rev. A. [Online]. 67(6) (2003, Jun.) 063203-063215. Available: https://doi.org/10.1103/PhysRevA.67.063203

[2] J. Jellinek, P.H. Acioli, *Magnesium clusters: structural and electronic properties and the size-induced nonmetal-to-metal transition*. J. Phys. Chem. A. [Online]. 106(45) (2002, Oct.) 10919-10925. Available: https://doi.org/10.1021/jp020887g

[3] I. Heidari, S. De, S. Ghazi, S. Goedecker, D. Kanhere, *Growth and Structural Properties of Mg N (N= 10–56) Clusters: Density Functional Theory Study*. J. Phys. Chem. A. [Online]. 115(44) (2011, Sep.) 12307-12314. Available: https://doi.org/10.1021/jp204442e

[4] S. Janecek, E. Krotscheck, M. Liebrecht, R. Wahl, *Structure of Mg n and Mg n+ clusters up to n= 30*. Eur. Phys. J. D. [Online]. 63 (2011, Jun.) 377-390. Available: https://doi.org/10.1140/epjd/e2011-10694-2

[5] A. Köhn, F. Weigend, R. Ahlrichs, *Theoretical study on clusters of magnesium*. Phys. Chem. Chem. Phys. [Online]. 3 (2001, Jan.) 711-719. Available: https://doi.org/10.1039/B007869G

[6] M. Monteverde, M. Nunez-Regueiro, N. Rogado, K. Regan, M. Hayward, T. He, S. Loureiro, R.J. Cava, *Pressure dependence of the superconducting transition temperature of magnesium diboride*. Science. [Online]. 292(5514) (2001, Apr.) 75-77. Available: https://doi.org/10.1126/science.1059775

[7] S. Er, G.A. de Wijs, G. Brocks, *Tuning the hydrogen storage in magnesium alloys*. J. Phys. Chem. Lett. [Online]. 1(13) (2010, Jun.) 1982-1986. Available: https://doi.org/10.1021/jz100386j

[8] R. Nevshupa, J.R. Ares, J.F. Fernández, A. del Campo, E. Roman, *Tribochemical decomposition of light ionic hydrides at room*

temperature. J. Phys. Chem. Lett. [Online]. 6(14) (2015, Jun.) 2780-2785. Available: https://doi.org/10.1021/acs.jpclett.5b00998

[9] G. Barcaro, R. Ferrando, A. Fortunelli, G. Rossi, *Exotic supported copt nanostructures: from clusters to wires*. J. Phys. Chem. Lett. [Online]. 1(1) (2009, Nov.) 111-115. Available: https://doi.org/10.1021/jz900076m

[10] L.-Y. Chen, J.-Q. Xu, H. Choi, M. Pozuelo, X. Ma, S. Bhowmick, J.-M. Yang, S. Mathaudhu, X.-C. Li, *Processing and properties of magnesium containing a dense uniform dispersion of nanoparticles*, Nature, 528 (2015, Dec.) 539-543. Available: https://doi.org/10.1038/nature16445

[11] J. Yoo, A. Aksimentiev, Improved parametrization of Li+, Na+, K+, and Mg2+ ions for all-atom molecular dynamics simulations of nucleic acid systems. J. Phys. Chem. Lett. [Online]. 3(1) (2011, Dec) 45-50. Available: https://doi.org/10.1021/jz201501a

[12] J. Jellinek, P.H. Acioli, *Magnesium Clusters: Structural and Electronic Properties and the Size-Induced Nonmetal-to-Metal Transition*. J. Phys. Chem. A. [Online]. 107(10) (2003, Feb.) 1670-1670. Available: https://doi.org/10.1021/jp0301655

[13] J. Akola, K. Rytkönen, M. Manninen, *Metallic evolution of small magnesium clusters*. Eur. Phys. J. D. [Online]. 16 (2001, Oct.) 21-24. Available: https://doi.org/10.1007/s100530170051

[14] E.R. Davidson, R.F. Frey, *Density functional calculations for Mg n+ clusters*. J. Chem. Phys. [Online]. 106(6) (1997, Jun.) 2331-2341. Available: https://doi.org/10.1063/1.473096

[15] X. Gong, Q. Zheng, Y.-z. He, *Electronic structures of magnesium clusters*. Phys. Lett. [Online]. A, 181(6) (1993, Nov.) 459-464. Available: https://doi.org/10.1016/0375-9601(93)91150-4

[16] V. Kumar, R. Car, *Structure, growth, and bonding nature of Mg clusters*. Phys. Rev.B. [Online]. 44(15) (1991, Oct) 8243-8255. Available: https://doi.org/10.1103/PhysRevB.44.8243

[17] X. Xia, X. Kuang, C. Lu, Y. Jin, X. Xing, G. Merino, A. Hermann, Deciphering the structural evolution and electronic properties of magnesium clusters: an aromatic homonuclear metal Mg17 cluster.

J. Phys. Chem. A. [Online]. 120(40) (2016, Sep.) 7947-7954. Available: https://doi.org/10.1021/acs.jpca.6b07322

[18] J. Lv, Y. Wang, L. Zhu, Y. Ma, *Particle-swarm structure prediction on clusters*. J. Chem. Phys. [Online]. 137(8) (2012, Aug.) 084104-084111. Available: https://doi.org/10.1063/1.4746757

[19] M. Brack, *The physics of simple metal clusters: self-consistent jellium model and semiclassical approaches*. Rev. Mod. Phys. [Online]. 65(3) (1993, Sep) 677-732. Available: https://doi.org/10.1103/RevModPhys.65.677

[20] W.A. De Heer, *The physics of simple metal clusters: experimental aspects and simple models*. Rev. Mod. Phys. [Online]. 65(3) (1993, Sep) 611-615. Available: https://doi.org/10.1103/RevModPhys.65.611

[21] K.S. John, K. Feyisayo, *Air pollution by carbon monoxide (CO) poisonous gas in Lagos Area Southwestern Nigeria*. J. Atmos. Clim. Sci. [Online]. 3(4) (2013, Aug.) 510-514. Available: http://dx.doi.org/10.4236/acs.2013.34053

[22] L. Wu, R. Wang, *Carbon monoxide: endogenous production, physiological functions, and pharmacological applications*. J. Pharmacol. Rev. [Online]. 57(4) (2005, Dec.) 585-630. Available: https://doi.org/10.1124/pr.57.4.3

[23] A. Nakao, H. Toyokawa, A. Tsung, M. Nalesnik, D. Stolz, J. Kohmoto, A. Ikeda, K. Tomiyama, T. Harada, T. Takahashi, Ex vivo application of carbon monoxide in University of Wisconsin solution to prevent intestinal cold ischemia/reperfusion injury. Am. J. Transplant. [Online]. 6(10) (2006, Jul.) 2243-2255. Available: https://doi.org/10.1111/j.1600-6143.2006.01465.x

[24] R. Motterlini, L.E. Otterbein, *The therapeutic potential of carbon monoxide*. Nat. Rev. Drug Discov. [Online]. 9 (2010, Sep) 728-743. Available: https://doi.org/10.1038/nrd3228

[25] J. Haggarty, K.E. Burgess, *Recent advances in liquid and gas chromatography methodology for extending coverage of the metabolome*. Curr. Opin. Biotech. [Online]. 43 (2017, Feb.) 77-85. Available: https://doi.org/10.1016/j.copbio.2016.09.006

[26] A. Masek, E. Chrzescijanska, M. Latos, A. Kosmalska, *Electrochemical and Spectrophotometric Characterization of the Propolis Antioxidants Properties*. Int. J. Electrochem. Sci. [Online]. 14 (2019, Jan.) 1231-1247. Available: https://doi.org/10.20964/2019.02.66

[27] A.M. Pisoschi, G.P. Negulescu, *Methods for total antioxidant activity determination: a review*. Biochem Anal Biochem. [Online]. 1(1) (2011, Oct) 106-115. Available: http://dx.doi.org/10.4172/2161-1009.1000106

[28] J.-S. Noh, J.M. Lee, W. Lee, *Low-dimensional palladium nanostructures for fast and reliable hydrogen gas detection*. Sensors. [Online]. 11(1) (2011, Jan.) 825-851. Available: https://doi.org/10.3390/s110100825

[29] S. Korniy, V. Pokhmurskii, V. Kopylets, *A theoretical study of CO adsorption on Pt–Me (Me–Fe, Co, Ni) nanoclusters*. J. Thermodyn. Catal. [Online]. 7(2) (2016, Jun.) 169-172. Available: http://dx.doi.org/10.4172/2157-7544.1000169

[30] M. Lu, R. Huang, W. Xu, J. Wu, M. Fu, L. Chen, D. Ye, *Competitive Adsorption of O2 and Toluene on the Surface of FeOx/SBA-15 Catalyst*. Aerosol Air Qual Res. [Online]. 17(9) (2017, Sep.) 2310-2316. Available: https://doi.org/10.4209/aaqr.2016.05.0186

[31] A.K. Mishra, A. Roldan, N.H. de Leeuw, *A density functional theory study of the adsorption behaviour of CO2 on Cu2O surfaces*. J. Chem. Phys. [Online]. 145(4) (2016, Jul.) 044709-044721. Available: https://doi.org/10.1063/1.4958804

[32] J. Schnadt, J. Knudsen, X.L. Hu, A. Michaelides, R.T. Vang, K. Reuter, Z. Li, E. Lægsgaard, M. Scheffler, F. Besenbacher, *Experimental and theoretical study of oxygen adsorption structures on Ag (111)*. Phys. Rev. B. [Online]. 80(7) (2009, Aug.) 075424-075435. Available: https://doi.org/10.1103/PhysRevB.80.075424

[33] B. Wanno, C. Tabtimsai, *A DFT investigation of CO adsorption on VIIIB transition metal-doped graphene sheets*. Superlattices Microstruct. [Online]. 67 (2014, Mar.) 110-117. Available: https://doi.org/10.1016/j.spmi.2013.12.025

[34] F. Azimi, E. Tazikeh-Lemeski, F. Kaveh, M. Monajjemi, *Optoelectronical Properties of a Metalloid-Doped B12N12 Nano-Cage*. J. Optoelectron. Nanostructures. [Online]. 5(1) (2020, Mar.) 101-119. Available: http://journals.miau.ac.ir/article_4036.html

[35] H.A. Al-Abadleh, V. Grassian, *FT-IR study of water adsorption on aluminum oxide surfaces*. Langmuir. [Online]. 19(2) (2002, Dec.) 341-347. Available: https://doi.org/10.1021/la026208a

[36] J.-K. Chen, S.-M. Yang, B.-H. Li, C.-H. Lin, S. Lee, *Fluorescence quenching investigation of methyl red adsorption on aluminum-based metal–organic frameworks*. Langmuir. [Online]. 34(4) (2018, Jan.) 1441-1446. Available: https://doi.org/10.1021/acs.langmuir.7b04240

[37] X.-J. Kuang, X.-Q. Wang, G.-B. Liu, *A density functional study on the adsorption of hydrogen molecule onto small copper clusters*. J. Chem. Sci. [Online]. 123 (2011, Sep.) 743-754. Available: https://doi.org/10.1007/s12039-011-0130-3

[38] Q.-M. Ma, Z. Xie, J. Wang, Y. Liu, Y.-C. Li, *Structures, binding energies and magnetic moments of small iron clusters: A study based on all-electron DFT*. Solid State Commun. [Online]. 142(1) (2007, Apr.) 114-119. Available: https://doi.org/10.1016/j.ssc.2006.12.023

[39] R. Hussain, A.I. Hussain, S.A.S. Chatha, A. Mansha, K. Ayub, *Density functional theory study of geometric and electronic properties of full range of bimetallic AgnYm (n+ m= 10) clusters*. J. Alloys Compd. [Online]. 705 (2017, May.) 232-246. Available: https://doi.org/10.1016/j.jallcom.2017.02.008

[40] S.F. Matar, *DFT study of hydrogen instability and magnetovolume effects in CeNi*. Solid State Sci. [Online]. 12(1) (2010, Jan.) 59-64. Available: https://doi.org/10.1016/j.solidstatesciences.2009.10.003

[41] S.J. Mousavi, First–Principle Calculation of the Electronic and Optical Properties of Nanolayered ZnO Polymorphs by PBE and mBJ Density Functionals. J. Optoelectron. Nanostructures. [Online]. 2(4) (2017, Dec.) 1-18. Available: http://journals.miau.ac.ir/article_2570.html

[42] H. Salehi, *Ab-initio study of Electronic, Optical, Dynamic and Thermoelectric properties of CuSbX2 (X= S, Se) compounds*. J.

Optoelectron. Nanostructures. [Online]. 3(2) (2018, Jun.) 53-64. Available: http://jopn.miau.ac.ir/article_2864.html

[43] S. Fotoohi, S. Haji Nasiri, *Vacancy Defects Induced Magnetism in Armchair Graphdiyne Nanoribbon*. J. Optoelectron. Nanostructures. [Online]. 4(4) (2019, Dec.) 15-38. Available: http://jopn.miau.ac.ir/article_3754.html

[44] M. Askaripour Lahiji, A. Abdolahzadeh Ziabari, *Ab–initio study of the electronic and optical traits of Na0. 5Bi0. 5TiO3 nanostructured thin film*. J. Optoelectron. Nanostructures. [Online]. 4(3) (2019, Sep.) 47-58. Available: http://jopn.miau.ac.ir/article_3619.html

[45] F. Weinhold, C.R. Landis, *Natural bond orbitals and extensions of localized bonding concepts*. Chem Educ Res Pract. [Online]. 2(2) (2001, May.) 91-104. Available: https://doi.org/10.1039/B1RP90011K

[46] S.J. Mousavi, *Ab-initio LSDA Study of the Electronic States of Nano Scale Layered LaCoO3/Mn Compound: Hubbard Parameter Optimization*. J. Optoelectron. Nanostructures. [Online]. 5(4) (2020, Dec.) 111-122. Available: http://jopn.miau.ac.ir/article_4512.html

[47] F. Biegler- König, J. Schönbohm, *Update of the AIM2000-program for atoms in molecules*. J. Comput. Chem. [Online]. 23(15) (2002, Nov.) 1489-1494. Available: https://doi.org/10.1002/jcc.10085

[48] R.D. Dennington, T.A. Keith, J.M. Millam, *GaussView 5.0. 8*, Gaussian Inc, 340 (2008).

[49] M.R. Dehghan, S. Ahmadi, Z.M. Kotena, M. Niakousari, *Adsorption of oxygen molecule on aromatic magnesium nanoclusters with centrality of Be, Mg, and Ca: a DFT study (peer review)*.

[50] T. Yanai, D.P. Tew, N.C. Handy, *A new hybrid exchange–correlation functional using the Coulomb-attenuating method (CAM-B3LYP)*. Chem. Phys. Lett. [Online]. 393(1) (2004, Jul.) 51-57. Available: https://doi.org/10.1016/j.cplett.2004.06.011

[51] M. Frisch, G. Trucks, H.B. Schlegel, G. Scuseria, M. Robb, J. Cheeseman, G. Scalmani, V. Barone, B. Mennucci, G. Petersson, *Gaussian 09, Revision B.01*, (Gaussian, Inc., Wallingford, CT, 2009).

[52] S.F. Boys, F. Bernardi, The calculation of small molecular interactions by the differences of separate total energies. Some procedures with reduced errors. Mol. Phys. [Online]. 19(4) (1970, Jun.) 553-566. Available: https://doi.org/10.1080/00268977000101561

[53] N.M. O'boyle, A.L. Tenderholt, K.M. Langner, *Cclib: a library for package- independent computational chemistry algorithms*. J. Comput. Chem. [Online]. 29(5) (2008, Apr.) 839-845. Available: https://doi.org/10.1002/jcc.20823

[54] T. Lu, F. Chen, *Multiwfn: a multifunctional wavefunction analyzer*. J. Comput. Chem. [Online]. 33(5) (2012, Feb.) 580-592. Available: https://doi.org/10.1002/jcc.22885

[55] M. Shahabi, H. Raissi, Investigation of the molecular structure, electronic properties, AIM, NBO, NMR and NQR parameters for the interaction of Sc, Ga and Mg-doped (6, 0) aluminum nitride nanotubes with COCl 2 gas by DFT study. J Incl Phenom Macro. [Online]. 84 (2016, Feb.) 99-114. Available: https://doi.org/10.1007/s10847-015-0587-7

[56] R.F. Bader, *Atoms in molecules*. Acc. Chem. Res. [Online]. 18(1) (1985, Jan.) 9-15. Available: https://doi.org/10.1021/ar00109a003

[57] M.D. Esrafili, H. Behzadi, *A DFT study on carbon-doping at different sites of (8, 0) boron nitride nanotube*. J. Struct. Chem. [Online]. 24 (2013, Apr.) 573-581. Available: https://doi.org/10.1007/s11224-012-0110-3

[58] I. Rozas, I. Alkorta, J. Elguero, *Behavior of ylides containing N, O, and C atoms as hydrogen bond acceptors*. J. Am. Chem. Soc. [Online]. 122(45) (2000, Nov.) 11154-11161. Available: https://doi.org/10.1021/ja0017864

[59] S. Ahmadi, V. ManickamAchari, Z. Hussain, R. Hashim, Epimeric and anomeric relationship of octyl-α-D-gluco/galactosides: Insight from density functional theory and atom in molecules studies. Comput. Theor. Chem. [Online]. 1108(15) (2017, May.) 93-102. Available: https://doi.org/10.1016/j.comptc.2017.03.023

[60] S. Ahmadi, V.M. Achari, H. Nguan, R. Hashim, Atomistic simulation studies of the α/β-glucoside and galactoside in anhydrous

bilayers: effect of the anomeric and epimeric configurations. J. Mol. Model. [Online]. 20 (2014, Mar.) 2165. Available: https://doi.org/10.1007/s00894-014-2165-0

[61] R.G. Pearson, *Absolute electronegativity and hardness: applications to organic chemistry*. J. Org. Chem. [Online]. 54(6) (1989, Mar.) 1423-1430. Available: https://doi.org/10.1021/jo00267a034

[62] Z. Zhou, R.G. Parr, *Activation hardness: new index for describing the orientation of electrophilic aromatic substitution*. J. Am. Chem. Soc. [Online]. 112(15) (1990, Jul.) 5720-5724. Available: https://doi.org/10.1021/ja00171a007

[63] R.G. Parr, P.K. Chattaraj, *Principle of maximum hardness*. J. Am. Chem. Soc. [Online]. 113(5) (1991, Feb.) 1854-1855. Available: https://doi.org/10.1021/ja00005a072

[64] R.G. Parr, R.G. Pearson, *Absolute hardness: companion parameter to absolute electronegativity*. J. Am. Chem. Soc. [Online]. 105(26) (1983, Dec.) 7512-7516. Available: https://doi.org/10.1021/ja00364a005

[65] R.G. Pearson, *Absolute electronegativity and absolute hardness of Lewis acids and bases*. J. Am. Chem. Soc. [Online]. 107(24) (1985, Nov.) 6801-6806. Available: https://doi.org/10.1021/ja00310a009